Journal of Quantitative Spectroscopy & Radiative Transfer 217 (2018) 459–473

Contents lists available at ScienceDirect

Journal of Quantitative Spectroscopy & Radiative Transfer

journal homepage: www.elsevier.com/locate/jqsrt

Light scattering and absorption by fractal aggregates including soot

Christopher M. Sorensen[a,*], Jérôme Yon[b], Fengshan Liu[c], Justin Maughan[a], William R. Heinson[d], Matthew J. Berg[a]

[a] Kansas State University, Department of Physics, 1228 N. 17th St., Manhattan, KS 66506-2601 USA
[b] CORIA-UMR 6614, Normandie Université, CNRS, INSA et Université de Rouen, Saint Etienne du Rouvray, France
[c] National Research Council, Measurement Science and Standards, 1200 Montreal Rd., Ottawa, Ontario K1A 0R6 Canada
[d] Washington University in St. Louis, Department of Energy, Environment and Chemical Engineering, 1 Brookings Drive, St. Louis, MO 63130-4899 USA

ARTICLE INFO

Article history:
Received 20 March 2018
Revised 17 May 2018
Accepted 17 May 2018
Available online 18 May 2018

Keywords:
Fractal aggregates
Scattering
Absorption
Soot
Rayleigh-Debye-Gans approximation

ABSTRACT

This paper addresses how well and under what conditions the Rayleigh-Debye-Gans (RDG) approximation describes scattering and absorption of light by fractal aggregates (FA) including soot. The RDGFA theory, which is the prevailing, first order description of this problem, has two assumptions: the monomers, or primary particles, of the aggregate scatter and absorb in the Rayleigh regime, and the aggregate scatters in the diffraction limit weighted by this Rayleigh scattering and absorbs as a system of independent monomer particles. The aggregates studied here are formed via Diffusion Limited Cluster Aggregation (DLCA) and have a fractal dimension $D = 1.78 \pm 0.04$ and prefactor of $k_0 = 1.35 \pm 0.10$. The aggregates are a collection of monodisperse spherical monomers with point contacts. Optical calculations were performed with the multiple sphere T-matrix (MSTM) and DDSCAT codes for incident light polarized perpendicular to the scattering plane. The scattering considered is the forward scattering intensity and the angular scattering as parameterized by the scattering wave vector. The total absorption cross section for aggregates is also calculated. This work stresses the systematic study of the effects of the variables of monomers per aggregate, which ranged from one to 502, two monomer size parameters of 0.157 and 0.314, and a wide range of refractive index real and imaginary parts. It also considers soot refractive indices with three representative dispersions. A summary of results for both scattering and absorption includes deviations from RDGFA theory ranging as large as 35% with positive deviations increasing with the real part of the refractive index and negative deviations growing with the imaginary part. These deviation from the RDG limit are shown to be similar to deviations for spheres.

1. Introduction

The problem of how fractal aggregates, and in particular soot fractal aggregates, scatter and absorb light is important in many applications ranging from in situ diagnostics of soot formation in flames to the effects of soot and other aggregates on the global environment. The conventional description for fractal aggregate absorption and scattering is a combination of the Rayleigh and Rayleigh-Debye-Gans (RDG) approximation. The Rayleigh approximation assumes that a monomer in the aggregate is sufficiently small that the incident field may be treated as static across the monomer. Meanwhile, the RDG assumes that the light interacts with the aggregate so weakly that scattering from any given monomer does not affect another monomer. Thus, there is no internal coupling within the aggregate in the RDG approximation, or equivalently, there is no internal multiple scattering. A consequence of this is that the aggregate's internal field is equal to the incident field modified by the Lorentz-Lorenz factor as shown in the appendix. A review of the RDG fractal aggregate (RDGFA) theory was given in [1], and the appendix here demonstrates how it emerges as a formal solution to the Maxwell equations under two approximations.

As with any theoretical description, the question arises how well and under what conditions does RDGFA work? This has been addressed extensively in the past. In general, the findings are that RDGFA can yield errors on the order of 10% or more depending, of course, on the various properties of the aggregate such as aggregate size, primary particle (or monomer) size, refractive index, and the fractal parameters. However, the variety of properties and conditions and the lack of extensive systematic studies have not led to a quantitative consensus description of the deviations. It is the purpose of this paper to provide such a description. Here the scattering of light with a polarization perpendicular to the scatter-

* Corresponding author.
E-mail address: sor@phys.ksu.edu (C.M. Sorensen).

https://doi.org/10.1016/j.jqsrt.2018.05.016
0022-4073/

ing plane will be calculated and compared to the RDGFA theory. The scattering considered will be the forward scattering intensity and the angular scattering as parameterized by the scattering wave vector. The total absorption cross section for aggregates will also be calculated and compared to RDGFA theory.

2. Fractal aggregates

The scaling relation between the number of monomers in the aggregate N and the linear size as specified by the radius of gyration R_g of the aggregate is [1]

$$N = k_0(R_g/a)^D \tag{1}$$

where D is the fractal dimension, k_0 is the scaling prefactor and a is the primary particle or monomer radius.

In this work we study aggregates created by diffusion limited cluster aggregation (DLCA) [2,3]. DLCA involves aggregates diffusing randomly through space, and then, if any two collide, they stick together irreversibly. This is perhaps the most common type of aggregation and represents well what happens in nature. The resulting DLCA aggregates have a fractal dimension of $D = 1.78 \pm 0.04$ with a prefactor of $k_0 = 1.35 \pm 0.10$ for a spatial dimension of $d = 3$ [4–6]. This DLCA morphology describes well the morphology of pristine soot.

3. Review

Sorensen [1] reviewed work up to 2001 that tested the RDGFA theory. Here we quote, "In summary, it appears that for DLCA ($D \simeq 1.8$) aggregates multiple scattering can affect the scattering and absorption cross sections by 10 to 20%. For small ka there is an enhancement which can cross over to a reduction if the refractive index has a significant imaginary part, as does soot. Fractal dimension > 2 can also see an eventual diminution of cross section as size increases." With this foundation, we now review more recent work.

A considerable amount of recent work supports these conclusions. Typically, aggregates have been created numerically using either DLCA simulations or tunable codes to tailor make the aggregates. Their exact radiative properties are then determined by using T-Matrix [7,8], GMM [9], and DDA methods [10,11].

Much of this work considered a wide range of variables including monomer size and size distribution [12,13], monomer size parameter [14,15], the number of monomers (from 1 to 1000) and incident wavelength (from 266 nm to 1064 nm) which caused the refractive index to vary via dispersion [16], refractive index [17] necking and overlap between monomers [18] and added coatings [19,20]. Here our goal is to return to the simple situation of one morphology, the DLCA morphology, and determine the functionalities with monomer size, aggregate size and refractive index by systematically varying these parameters.

4. Light scattering

4.1. Diffraction

A useful point of view to understand and describe light scattering by particles is to apply light's wave nature first and then add its electromagnetic character slowly. With minimal electromagnetic character, achieved by having a refractive index such that $|m-1| \ll 1$, diffraction describes the scattering pattern. With increasing electromagnetic character, the scattering pattern systematically evolves away from the diffraction limit.

We represent the wave amplitude $E(\mathbf{r})$ at position vector $\mathbf{r}$ in the customary, complex notation

$$E(\boldsymbol{r}) = e^{i\boldsymbol{k}\cdot\boldsymbol{r}} \tag{2}$$

where $\mathbf{k}$ is the wave vector with amplitude $k = 2\pi/\lambda$ and λ is the wavelength of light. The diffracted wave at the detector is

$$E(q) \sim \int n(\boldsymbol{r}) e^{i\boldsymbol{q}\cdot\boldsymbol{r}} d\boldsymbol{r} \tag{3}$$

In Eq. (3) n($\mathbf{r}$) is the matter density profile of the scattering object, and $\mathbf{q}$ is the scattering wave vector given by

$$\boldsymbol{q} = \boldsymbol{k}_{inc} - \boldsymbol{k}_{sca} \tag{4}$$

where $\mathbf{k}_{inc}$ and $\mathbf{k}_{sca}$ are the incident and scattering wave vectors, respectively. The magnitude of the scattering wave vector is

$$q = (4\pi/\lambda)\sin(\theta/2) \tag{5}$$

In Eq. (5) θ is the angle between the incident and scattering wave vectors; it is the scattering angle. Note that Eq. (3) has the form of a Fourier transform with the physically inspired q as the Fourier variable.

The scattered intensity is the square of the scattered field, thus

$$I(q) \sim \left| \int n(\boldsymbol{r}) e^{i\boldsymbol{q}\cdot\boldsymbol{r}} d\boldsymbol{r} \right|^2 \tag{6}$$

Eq. (6) yields an intensity that has been averaged over all orientations of the object. With this, one can define a structure factor S(q) with any of a few different normalizations. If one imagines the scattering object as divided into N infinitesimal sub-volumes, S(q) can be defined as

$$S(q) = N^{-2} \left| \int n(\boldsymbol{r}) e^{i\boldsymbol{q}\cdot\boldsymbol{r}} d\boldsymbol{r} \right|^2 \tag{7}$$

Note that S(0) = 1. Application of the convolution theorem yields

$$S(\boldsymbol{q}) = \int g(\boldsymbol{r}) e^{i\boldsymbol{q}\cdot\boldsymbol{r}} d\boldsymbol{r} \tag{8}$$

where

$$g(\boldsymbol{r}) = N^{-2} \int n(\boldsymbol{u}) n(\boldsymbol{r}-\boldsymbol{u}) d\boldsymbol{u} \tag{9}$$

is a convolution of $n(\boldsymbol{r})$ with itself, better known as the density autocorrelation function.

One can then summarize and say that the structure factor is the normalized diffraction pattern scattered from the object. Furthermore, the structure factor and the density autocorrelation functions are Fourier transform pairs and hence carry the same structural information. However, their view points are in reciprocal spaces: real space and q-space.

4.2. The RDG limit

In the section above diffraction was derived using the situation where incident waves scattered from the sub-volumes of the scattering object went directly to the detector and did not interact with other sub-volumes of the scattering object. This is clearly an idealization. The situation in which there is scattering from one sub-volume to another has internal coupling and, equivalently, is said to have internal multiple scattering. This situation typically occurs when the refractive index m of the object is significantly greater than one (see Section 4.3). In the RDG limit the refractive index is small hence there is no multiple scattering between monomers, and consequently, the internal field is related to, but as shown below, is nevertheless not equal to the incident field. Then, the angular scattering pattern is approximately described by the diffracted structure factor. However, the magnitude of the scattering is not specified until light's electromagnetic character is included in the formulation. The weakest way to include electromagnetism is to multiply the structure factor by the Rayleigh scattering cross section for the object (regardless of the size of the object). When this is done, the scattering is in the RDG limit. Then the scattered intensity in the RDG limit can be written conceptually as

$$Rayleigh\text{-}Debye\text{-}Gans\ (RDG)\ =\ S\ (q)\ x\ Rayleigh\ Scattering \quad (10)$$

A derivation of this result for the forward scattering direction is given in Section 9.

4.2.1. The RDG limit for spheres

As an example that will be useful below, consider scattering by a sphere. The structure factor for a sphere of radius a is

$$S(q) = \left[\frac{3}{u^3}(\sin u - u\cos u)\right]^2 \quad (11)$$

where $u = qa$, a dimensionless variable. The differential scattering cross section in the Rayleigh limit, $ka << 1$, for incident light polarized perpendicular to the scattering plane is

$$\frac{dCsca}{d\Omega} = k^4 a^6 F(m) \quad (12)$$

where

$$F(m) = \left|\frac{m^2-1}{m^2+2}\right|^2 \quad (13)$$

is the square of the Lorentz-Lorenz factor and $m = n + i\kappa$ is the complex index of refraction. Thus by Eq. (10) scattering by a sphere in the RDG limit is

$$\frac{dC_{sca}}{d\Omega} = k^4 a^6 F(m)\left[\frac{3}{u^3}(sinu - ucosu)\right]^2 \quad (14)$$

The scattered intensity at a given angle is proportional to the differential cross section. We will use the term "I_{Ray}" for the scattering that would come from a particle in the Rayleigh limit, proportional to Eq. (12). Then, for simplicity we will write

$$I(u)_{RDG} = I_{Ray}\left[(3/u^3)(sinu - ucosu)\right]^2 \quad (15)$$

It is important to recognize that Eq. (15) can apply for any size sphere even though the Rayleigh portion of it, Eq. (12), holds only when the size parameter $ka << 1$ when used by itself. Application of Eq. (15) to spherical particle scattering is called the RDG approximation.

Eq. (15) holds for light scattering when the combination of size and refractive index is small. The parameter that describes this combination will be explained below.

4.2.2. The RDG limit for aggregates

For many fractal aggregates, and especially soot, the condition $|m-1| \ll 1$ is not satisfied by the primary particles, the monomers, of the aggregate. However, the monomers are typically small so that they scatter in the Rayleigh limit. Given this the RDG approximation for fractal aggregates is that each monomer sees only the incident wave. Simulations of the internal wave within an aggregate's monomers show deviations 25% and larger relative to the incident wave [21]. Despite this deviation, that work also shows that the scattering pattern *does* agree well with RDG due to averaging over random aggregate-orientations. Moreover, RDG agrees with the scattering patterns observed in the laboratory, where randomly oriented aggregates are involved. These reasons motivate the use of the RDG here. Application of the RDG limit to aggregates is called RDG fractal aggregate (RDGFA) theory. Formally, the RDG limit holds when $|m-1| \ll 1$ and $2ka|m-1| \ll 1$. The theory predicts the scattering at a given angle θ is proportional to the monomer differential scattering cross section. However, it is usually assumed that the monomers are small so that this cross section is angle independent when the polarization is perpendicular to the scattering plane. The aggregate scattered waves in the forward direction, defined by $q < R_g^{-1}$, from all N monomers add in phase to yield a scattered intensity proportional to N^2. In non-forward directions, the relative phases of the monomer scattered waves are accounted for by the aggregate structure factor, S(q). Thus the RDG differential scattering cross section for an aggregate is [1]

$$\frac{dC_{sca}^{agg}}{d\Omega}(q) = N^2 \frac{dC_{sca}^{m}}{d\Omega} S(q) \quad (16)$$

where $\frac{dC_{sca}^{m}}{d\Omega}$ is the monomer differential scattering cross section. Note that $S(0) = 1$. If the monomers are in the Rayleigh regime, Eq. (12) applies. Combining Eqs. (12) and (16) yields

$$I(q) = \frac{dC_{sca}^{agg}}{d\Omega}(q) = N^2 k^4 a^6 F(m) S(q) \quad (17)$$

The first equality in Eq. (17) holds for incident light of unit intensity scattering one unit of distance from the aggregate to the detector. We include this so that we can use the simple notation of scattered intensity. It is possible to arrive at Eqs. (16) and (17) through the rigorous formalism of the Maxwell volume integral equation as shown in the appendix. Doing so is useful because it illustrates how the internal field in each monomer is connected to the aggregate's scattered intensity and highlights the role of the two approximations that are required to arrive at Eq. (16).

In this work we are concerned with rotationally averaged DLCA aggregates which have a monomer-monomer pair correlation function that is well described by a Gaussian cutoff [6,22,23]. This leads to, via the Fourier transformation, the structure factor

$$S(q) = \exp\left[-\left((qR_g)^2/D\right)\right] F_{1,1}\left[\frac{3-D}{2},\ \frac{3}{2};\ -\frac{(qR_g)^2}{D}\right] \quad (18)$$

where $F_{1,1}$ is the Kummer or Hypergeometric function. This equation expands to yield

$$S(q)\ \simeq 1 - (qR_g)^2/3 \quad when\ qR_g\ < 1 \quad (19)$$

$$S(q) = C(qR_g)^{-D}\ when\ qR_g\ > 1 \quad (20)$$

Eq. (19) is the Guinier result. The coefficient C in Eq. (20) is related to the prefactor by $C = 1.35/k_0$ and the prefactor is related to the stretching exponent of the monomer-monomer pair correlation function. This exponent is 2 for the Gaussian cutoff to yield $k_0 = 1.35\ \pm 0.05$. Thus, $C = 1.0\ \pm 0.04$ for the Gaussian cutoff structure factor.

Analysis of absorption in the RDG limit uses the facts that each of the N monomers sees only the incident light independent of all the other monomers in the aggregate and that absorption is a scalar process hence is not affected by phase. Thus, the total absorption cross section is simply N times the monomer absorption cross section

$$C_{abs}^{agg} = NC_{abs}^{m} \quad (21)$$

If the monomers are in the Rayleigh regime,

$$C_{abs}^{m} = 4\pi ka^3 E(m) \quad (22)$$

where

$$E(m) = Im\left[\frac{m^2-1}{m^2+2}\right] \quad (23)$$

4.3. The internal coupling parameter

In past work we have shown for variety of particle shapes including spheres that the evolution of scattering away from the RDG limit is controlled by the internal coupling parameter [24–27]. The general expression for the internal coupling parameter for any shape is [28]

$$\rho' = 2\pi k \frac{V}{A_{proj}} |\alpha(m)| \tag{24}$$

In the equation above V is the volume of the particle, $\alpha(m)$ is the average volume polarizability which is dependent on the both m and the shape or the particle, and A_{proj} is the orientationally averaged projected area. A favorable attribute of the internal coupling parameter is that it combines size parameter and refractive index into one parameter.

For spheres [29]

$$|\alpha(m)|_{sphere} = \frac{3}{4\pi} \left| \frac{(m^2-1)}{(m^2+2)} \right|. \tag{25}$$

Then Eq. (24) leads to the internal coupling parameter for scattering by a sphere as

$$\rho' = 2ka \left| \frac{m^2-1}{m^2+2} \right| \tag{26}$$

This parameter is similar to the well-known phase shift parameter, which for spheres is $\rho = 2ka|m-1|$, [29,30], but is more effective in its parameterization powers.

For an aggregate with N spherical monomers of radius a we now propose

$$V = N\left(\frac{4\pi}{3}\right)a^3 \tag{27}$$

$$A_{proj} = N^{0.92}\pi a^2 \qquad \text{for large N} \tag{28}$$

Eq. (28) is an empirical result found in many situations from TEM observations [31–33] to mobility considerations for DLCA aggregates [34,35]. Substitution of (27) and (28) into (24) leads to an expression for the internal coupling parameter for scattering by a DLCA aggregate (the exponent 0.92 is specific to DLCA aggregates)

$$\rho_{agg}{}' = N^{0.08}\rho'_{mon} \tag{29}$$

Given the success of ρ' in parameterizing scattering by other objects, we will test Eq. (29) for fractal aggregates below.

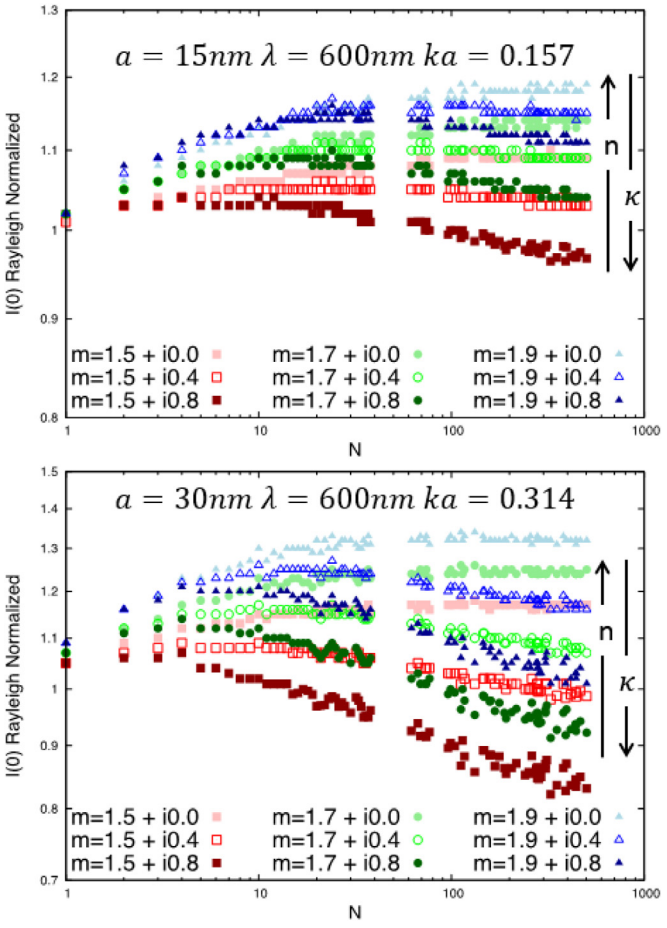

Fig. 1. Rayleigh normalized forward scattered intensity versus the number of monomers in the aggregate N for DLCA aggregates composed of monomers with size parameters of $ka = 0.157$ (top) and 0.314 (bottom). The monomers have a variety of refractive indices as indicated in the legend. Arrows to the far right indicate functionality trends with the real and imaginary parts of the refractive index, n and κ, respectively.

5. Calculation methods

In this work we created fractal aggregates by two different methods: the classic DLCA simulation algorithm described above and an algorithm [36,37]that can tailor-make aggregates with specified D and k_0.

The DLCA simulation algorithm used in this paper to create fractal aggregates was an off-lattice simulation with 10^6 monomers that were randomly placed in a three dimensional box. The box size was set so that the desired monomer volume fraction of $f_v = 0.001$ was obtained. At the beginning of each time step, the number of aggregates (N_c) was counted (note that the number of monomers was included in N_c). A random aggregate was chosen and time was incremented by N_c^{-1}. The probability that the aggregate is moved was inversely proportional to that aggregate's radius of gyration ($p \propto R_g^{-1}$) and was normalized so that monomers have $p = 1$. Results are applicable in the continuum limit where the frictional drag is given by the Stokes–Einstein expression with a drag proportional to the radius of gyration. The resulting DLCA aggregates have a fractal dimension of $D = 1.78 \pm 0.04$ with a prefactor of $k_0 = 1.35 \pm 0.10$ for a spatial dimension of $d = 3$ [4–6].

The tailor made fractal aggregates were generated using a two-step algorithm described in [36,8,37]. In the first step, a large number of different-sized small aggregates containing up to 31 primary particles were created using the tunable particle-cluster aggregation (PCA) algorithm. In the second step, larger fractal aggregates were built by using the tunable cluster-cluster aggregation (CCA) algorithm that merges two small aggregates generated in the first step by PCA at a time. Repeated application of CCA to two smaller aggregates produces even larger aggregates and this process continues until the desired number and size of fractal aggregates were obtained.

All orientationally averaged light scattering calculations for the aggregates were performed using a well-known and widely used multiple sphere T-matrix code (MSTM) developed by Mackowski and Mishchenko [38]. The MSTM calculates the electromagnetic properties of a group of spheres which may be located externally or internally to one another if the surfaces do not overlap. As aggregates are often modeled as a collection of spherical monomers, the MSTM code is ideally suited for calculating the light scattering properties of aggregates. Results presented in Section 8 have been determined by DDA approach (DDSCAT code version 7.3.2) [39] . For this purpose, particles are discretized polarizable elementary dipoles. In the present case, the dipolar density (mean number of dipoles per primary sphere diameter) is fixed to 10, ensuring a reliable determination of the radiative properties. The Maxwell equations are solved by considering the dipole coupling. The calculations were performed in the visible spectrum with a variety of refractive indices, respecting the accuracy criterion $|m|kd < 0.5$. The cross sections are averaged over one thousand orientations.

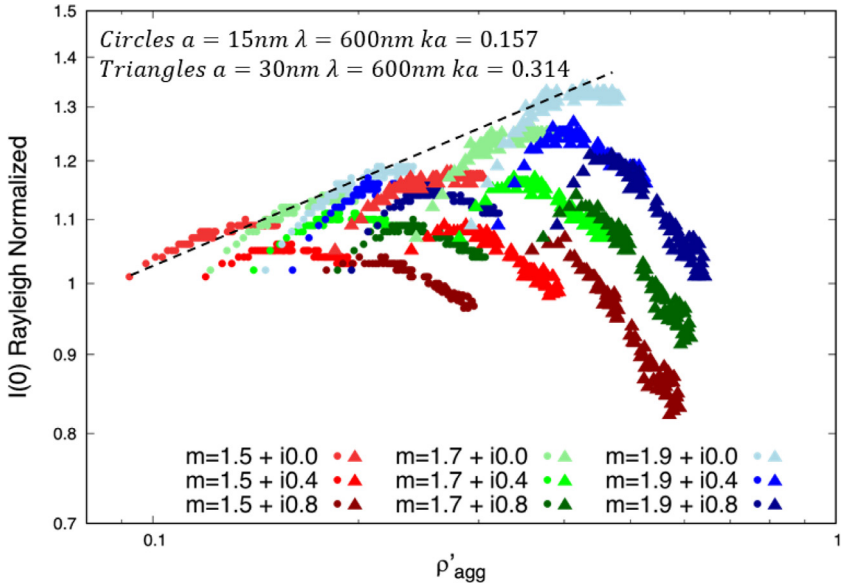

Fig. 2. Rayleigh normalized forward scattered intensity versus the aggregate internal coupling parameter ρ'_{agg} for DLCA aggregates composed of monomers with size parameters of $ka = 0.157$ (circles) and 0.314 (triangles). The monomers have a variety of refractive indices as indicated in the legend. The number of monomers per aggregate N ranges from 1 to 502. The dashed line indicates the trend when the imaginary part of the refractive index is $\kappa = 0$.

6. Comparisons to RDG

Our purpose here is to compare light scattering and absorption by aggregates of arbitrary size and refractive index to the RDGFA description. Deviations are expected with increasing refractive index (as we "turn on" the electromagnetic character of the light), monomer size parameter ka, and the overall size of the aggregate, which we will designate by the number of monomers per aggregate N. The structural parameters of fractal dimension and prefactor are also likely to be important, but in this work we limit the aggregates to be DLCA thus these two parameters are fixed.

The deviations of scattering and absorption from RDGFA theory will be represented by the ratios

$$I(0)\text{Rayleigh Normalized} = I(0)/N^2k^4a^6F(m), \tag{30}$$

$$I(q)\text{Rayleigh Normalized}/S(q) \tag{31}$$

and

$$C_{abs}\text{Rayleigh Normalized} = C_{abs}/N4\pi ka^3E(m) \tag{32}$$

Relations (30) and (31) compare the light scattering to the RDG limit in the forward direction and the entire q-range (hence angular range) to the RDG limit, respectively, whereas Eq. (32) compares the light absorption to the RDG limit. The denominators of Eqs. (30) and (32) are the RDGFA theory as obtained from Eqs. (17), with $S(0) = 1$, and (21) and (22), respectively. The ratios in Eqs. (30) and (32) were designated as A and h, respectively, by Yon, Liu and coworkers [12,16,18,20].

7. Aggregates with systematic variation of the refractive index

7.1. Forward scattering functionality *vs* N

Fig. 1 shows the Rayleigh normalized forward scattered intensity (the ratio of the forward scattered intensity to the RDGFA theory) Eq. (30), for DLCA aggregates versus the number of monomers per aggregate, N, for monomer radii of $a = 15$ and 30 nm scattering $\lambda = 600$ nm light, hence monomer size parameters $ka = 0.157$ and 0.314, respectively. If the ratio is not equal to one, the scattering deviates from the RDGFA theory. These plots show a weak functionality of the deviation with N as well as functionalities on refractive index and size parameter. In general the larger monomer size parameter shows larger variations of the normalized intensities of approximately +30% to −20% than the smaller size parameter with deviations of approximately +20% to −5%. The plots also show that the real part of the refractive index tends to cause positive deviations from unity whereas the imaginary part tends to cause negative deviations and these two can counteract each other. Note that the random fluctuations here and in similar figures below are due to the statistical nature of the aggregates.

7.2. Scattering functionality *vs* ρ'

The results in Fig. 1 are replotted in Fig. 2 versus ρ'_{agg} to discern whether or not this parameter can provide a universal description for the deviations of the forward scattering from the RDG limit. Recognize that for fixed refractive index m and size parameter ka the variation in ρ'_{agg} is due to the change in N, and because the functionality is $N^{0.08}$, the resulting range is small, a factor of $502^{0.08} = 1.64$.

Fig. 2 shows that when the imaginary part of the refractive index is $\kappa = 0$, the data for all real parts n and size parameters ka roughly line up to indicate some success for ρ'_{agg} as a universal parameter. However, inclusion of finite κ shows systematic trends to decrease the Rayleigh normalized forward intensity and the trends are not unified by ρ'_{agg}.

Fig. 2 leads us to question the behavior of the deviations for a very broad range of ρ'. Such a broad range would be very difficult to achieve by variation of N because the functionality is so weak. Thus to explore the functionality further and over a broader range more calculations were performed by varying the monomer size over the range $4 \le a \le 153$ nm hence the size parameter of the monomers over the range $0.042 \le ka \le 1.60$ when $\lambda = 600$ nm.

Fig. 3 (bottom) shows the deviations for N = 37, 104 and 205 aggregates vs ρ'_{agg} which ranges over two orders of magnitude from 0.03 to 3. A distinctive pattern, hinted at in Fig. 2, appears. For small ρ'_{agg} the ratios approach one. Then, with increasing ρ'_{agg}, the deviations increase and disperse with different refractive indices. The deviations are greater than one increasing with the refractive

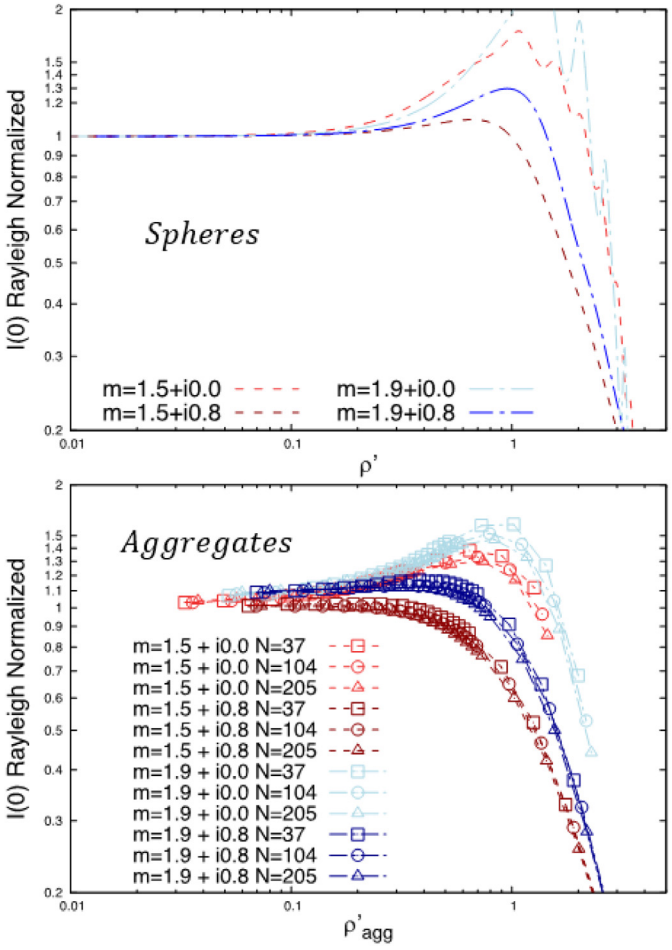

Fig. 3. Rayleigh normalized forward scattered intensity for: top, spheres, and bottom, DLCA aggregates, versus the internal coupling parameter ρ'. The DLCA aggregates were composed of $N = 37$, 104 and 205 monomers per aggregate with a monomer size parameter range of $0.042 \leq ka \leq 1.60$. The aggregates and spheres have the same set of refractive indices.

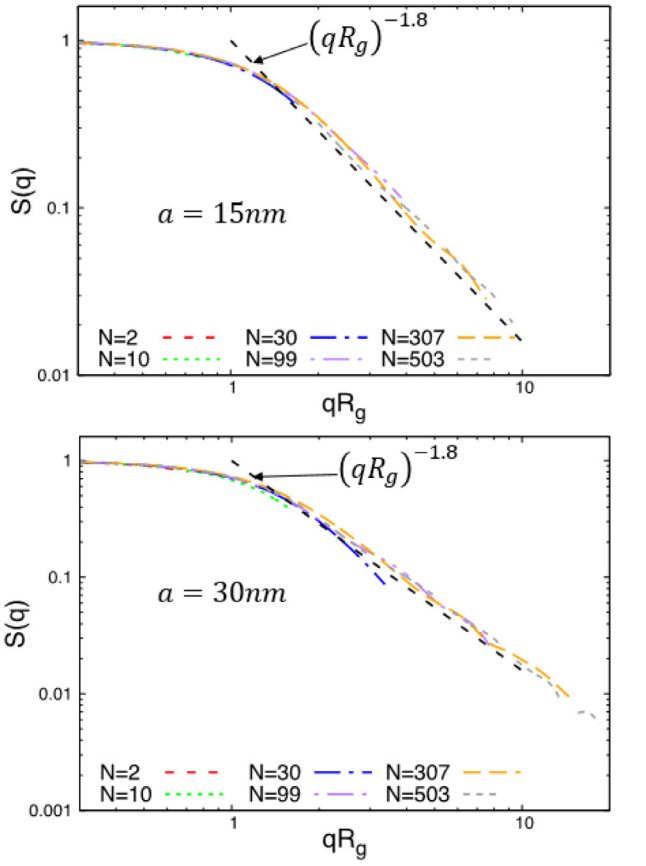

Fig. 4. Structure factors, S(q), for DLCA fractal aggregates of various number of monomers, N, versus qR_g. The monomer radii are $a = 15$ nm (upper) and 30 nm (lower). The marked black, dashed line in each plot shows the functionality $C(qR_g)^{-D}$ of Eq. (20) with $C = 1.0$ and fractal dimension $D = 1.8$.

index real part n but decreasing with the refractive index imaginary part κ. When $\rho'_{agg} \gtrsim 1$, the deviations begin a precipitous decrease which is limiting to a ρ'^{-2}_{agg} functionality.

Fig. 3 compares the behaviors with ρ' of aggregates and spheres to find very similar behavior; they are semi-quantitatively the same. There one sees the same approach to one at small ρ', substantial functionality with refractive index when $0.3 \leq \rho' \leq 3$, and then a precipitous decrease, independent of refractive index for each shape, when $\rho' \geq 1$ with a power law of ρ'^{-2}. The similarity suggests the same cause. Of course, when ρ' is small, the internal coupling, i.e., the internal multiple scattering, is negligible, so the internal field is equal to the incident field screened by the Lorentz-Lorenz factor and the RDG limit holds for both aggregates and spheres. As ρ' increases, the internal field is initially enhanced beyond the incident field so the scattered intensity is larger. This enhancement should be larger for larger refractive index real part and smaller with larger internal absorption which is dependent on the imaginary part of the refractive index. These dependencies are, in fact, seen. Ultimately, as ρ' grows past three, the internal coupling becomes so strong that the phase relationships between waves from different parts of the scatterer become complex so that destructive interference ensues to cause the drastic decrease in the forward scattering intensity. A similar behavior has been observed for scattering by a wide variety of ice crystal shapes [25].

7.3. Scattering functionality vs q

The RDG limit for the q-functionality (hence angular functionality) is the normalized structure factor S(q) of Eq. (10) with a particular functional form given in Eq. (18) valid for a Gaussian cutoff pair correlation function. Here we did not assume Eq. (18) is correct but instead calculated S(q) by Fourier transforming the real space structure of the DLCA aggregates formed in our simulations using Eq. (7). These Fourier transforms were orientationally averaged. The results are shown in Fig. 4.

The results in Fig. 4 show the classic behavior with a Guinier regime near $qR_g \simeq 1$ followed by a power law with slope equal to the fractal dimension. Note that the coefficient of the power law C, Eq. (20), is slightly larger than 1.0 for the smaller monomers. This occurs because individual aggregates will have different anisotropies hence different values of C than the ensemble average [6].

Figs. 5 and 6 show the Rayleigh normalized light scattering q-functionality across the entire angular range, from near zero to 180°. These figures also compare the light scattering to the structure factor via their ratio as described in relation (31). The difference between these two figures is that the monomer refractive index in Fig. 5 has no imaginary part while that in Fig. 6 has a significant value of $\kappa = 0.8$. Note that the ratio of relation (31) is a test of the applicability of the RDG limit for describing light scattering by these aggregates; it is a test of the RDGFA theory.

Inspection of these figures shows that light scattering does not significantly affect the shape of the plots. Furthermore, to a good approximation the Rayleigh normalized scattering ratio to the

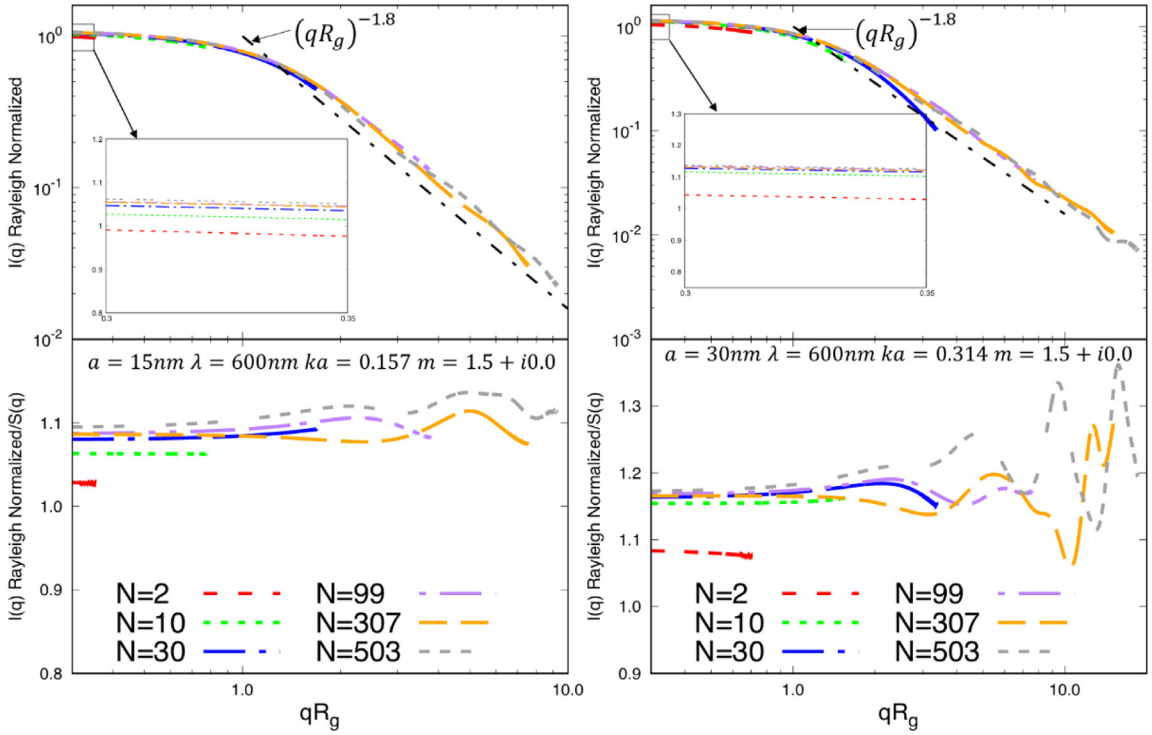

Fig. 5. Upper graphs: Rayleigh normalized scattered intensity for DLCA fractal aggregates of various number of monomers, N, versus qR_g. The monomer index of refraction is $m = 1.5 + i0.0$ and the size parameters are $ka = 0.157$ (left plot) and 0.314 (right). The marked, black, dot-dashed line in each plot shows the functionality $C(qR_g)^{-D}$ of Eq. (20) with C = 1.0 and fractal dimension D = 1.8. The insets show the behavior for very small qR_g, hence essentially I(0), Rayleigh normalized, the same information given in Fig. 1. Lower graphs: Rayleigh normalized scattered intensity divided by the structure factor, ratio (31), calculated using Eq. (7).

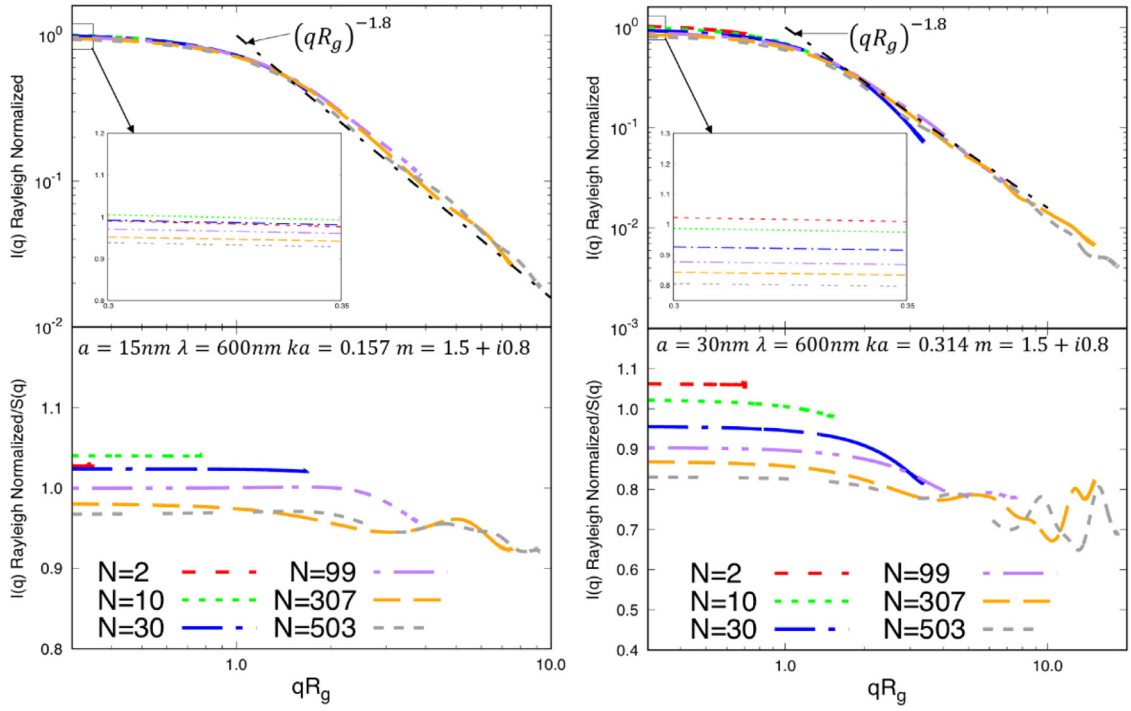

Fig. 6. Upper graphs: Rayleigh normalized scattered intensity for DLCA fractal aggregates of various number of monomers, N, versus qR_g. The monomer index of refraction is $m = 1.5 + i0.8$ and the size parameters are $ka = 0.157$ (left plot) and 0.314 (right). The marked, black, dot-dashed line in each plot shows the functionality $C(qR_g)^{-D}$ of Eq. (20) with C = 1.0 and fractal dimension D = 1.8. The insets show the behavior for very small qR_g, hence essentially I(0), Rayleigh normalized, the same information given in Fig. 1. Lower graphs: Rayleigh normalized scattered intensity divided by the structure factor, ratio (31), calculated using Eq. (7).

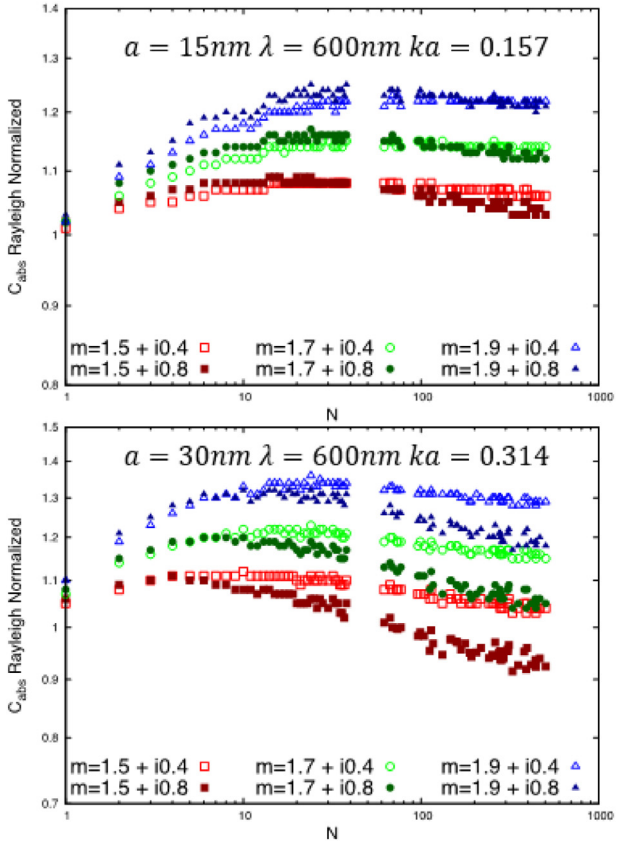

Fig. 7. Rayleigh normalized absorption cross section versus the number of monomers in the aggregate N for DLCA aggregates composed of monomers with size parameters of $ka = 0.157$ (top) and 0.314 (bottom). The monomers have a variety of refractive indices as indicated in the legend.

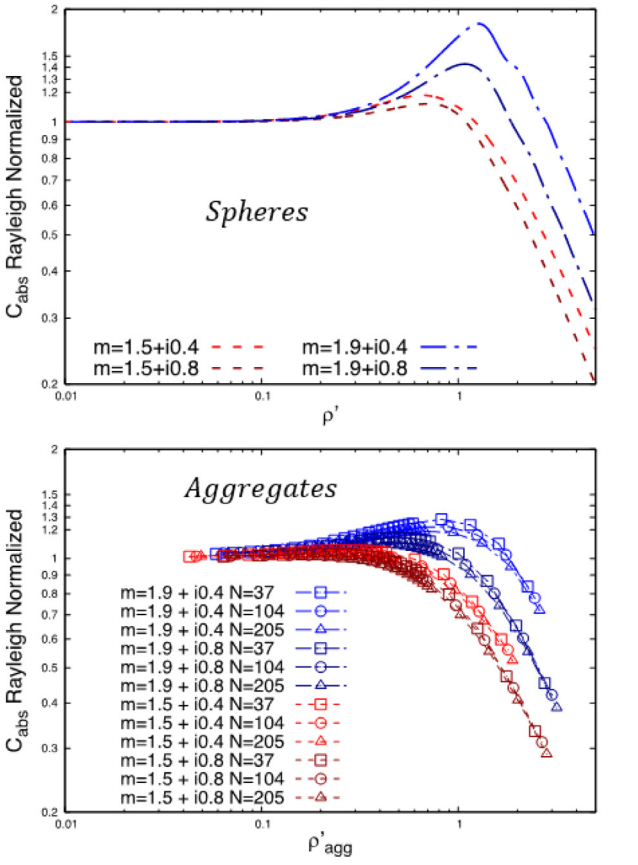

Fig. 8. Rayleigh normalized absorption cross sections versus the internal coupling parameter ρ' for: top, spheres, and bottom, DLCA aggregates. The DLCA aggregates were composed of $N = 37$, 104 and 205 monomers per aggregate with monomer size parameters in a range of $0.042 \leq ka \leq 1.60$. The aggregates and spheres have the same set of refractive indices.

structure factor is fairly uniform as a function of q with values near unity when $\kappa = 0.8$ to 10 to 20% larger when $\kappa = 0.0$. However, when $\kappa = 0.8$, the ratio in the power law regime shows a small but uniform decrease with increasing qR_g of about 10% or 20% for $ka = 0.157$ or 0.314, respectively. Because the ratio is decreasing with increasing qR_g, the slope in the power law regime in the upper plot will increase in magnitude and thereby cause the inferred fractal dimension from a light scattering experiment to be 2.5% to 5% larger than the true value. This effect was first noticed by Brasil et al. [40] and later by Liu et al. [41] and Yon et al. [16] for soot and is discussed further in Section 8.1.3, below.

7.4. Absorption functionality *vs* N

Fig. 7 shows the Rayleigh normalized absorption cross section (the ratio of the aggregate absorption cross section to the RDG limit), Eq. (32), for DLCA aggregates versus the number of monomers per aggregate, N, for monomer radii of $a = 15$ and 30 nm and $\lambda = 600$ nm light, hence monomer size parameters $ka = 0.157$ and 0.314, respectively. If the ratio is not equal to one, the aggregate absorption deviates from the RDGFA theory. These plots show a weak functionality of the Rayleigh normalized absorption cross section with N as well as functionalities on refractive index and size parameter similar to the Rayleigh normalized forward scattering behavior of Fig. 1. In general the smaller size parameter displays smaller variations of the normalized absorbances of approximately +5% to 25% than the larger size parameter of approximately −8% to +33%. The plots also show that the real part of the refractive index tends to cause positive deviations from unity whereas the imaginary part tends to cause negative deviations and these two can counteract each other. This behavior is similar to that for the Rayleigh normalized forward scattering.

7.5. Absorption functionality *vs* ρ'

Detailed plots of the Rayleigh normalized absorption cross section versus ρ'_{agg} similar to Fig. 2 did not show a conclusive unification. Nevertheless, Fig. 8 shows the Rayleigh normalized absorption cross section versus ρ'_{agg} over the same broad range of $0.03 \leq \rho'_{agg} \leq 3$ used in our study of the scattering, Fig. 3 above, for N = 37, 104 and 205 aggregates. A distinctive pattern similar to Fig. 3 appears. For small ρ'_{agg} the ratios approach one, i.e., no deviations from the RDGFA theory. Then, with increasing ρ'_{agg} the deviations disperse depending on the refractive index. The deviation increases with the refractive index real part n and decreases with the refractive index imaginary part κ. When $\rho'_{agg} \geq 1$, the deviations begin a precipitous decrease which is limiting to a ρ'^{-1}_{agg} functionality.

Fig. 8 shows that the behavior of the normalized absorption cross section with ρ' for aggregates and spheres is very similar. As for scattering, aggregate and sphere behaviors are semi-quantitatively the same. Once again we argue that as the internal field evolves away from the incident field that occurs when $\rho' \ll 1$, it first grows brighter with increasing ρ' and the real part of the refractive index n when $\rho' \geq 1$. Apparently, this enhanced internal field leads to an enhanced ability to absorb light.

Next we suggest an explanation of the absorption cross section for $\rho' \geq 1$. The size parameter of the spheres ka, where a is

the radius of the sphere, is approximately half the value of ρ' for the refractive indices used here. Thus when $\rho' \geq 1$, $ka \geq 0.5$. We have shown that a fundamental parameter to describe absorption by a sphere is κka, which is the ratio of the sphere radius to the penetration depth of the light [42]. Note that for $\kappa = 0.4$ and 0.8 $\kappa\ ka \geq 0.5$ when $\rho' \geq 1$. This means that absorption is just beginning to be significant at this point, and this is consistent with Fig. 7. This argument can be made semi-quantitative by using the result that the absorption cross section is proportional to the volume of the object in the Rayleigh limit for any shape. Also, if κka $\gtrsim$1, only the front part of the object will be illuminated. The approximate volume of this front part is the light penetration depth, $1/\kappa$k, times the cross sectional area, a^2, to yield a^2/κk. This ratioed by the volume of the object, a^3, yields $1/\kappa$ka $\sim \rho'^{-1}$, which is the functionality observed for both the sphere and the aggregate.

8. Aggregates with soot-like constant refractive index

8.1. Light scattering

The results above are a systematic study of scattering and absorption by DLCA fractal aggregates with direct comparisons to the RDG limit. We now focus specifically on soot with DLCA fractal morphology by using the refractive index of soot.

The refractive index of soot has seen a great many measurements by numerous workers in the previous decades. To start we will use two values that have seen considerable use in the literature. The first is related to the Dalzell and Sarofim value $m = 1.57 + i0.56$ [43] which is often rounded off to $m = 1.6 + i0.6$. The second is the value given by Smith [44] and in the review by Bond and Bergstrom [45] that has become popular, $m = 1.9 + i0.79$, which we round off to $1.9 + i0.8$. Note that we first consider fixed wavelength hence no refractive index dispersion.

Fig. 9 shows the deviations of the light scattering from the RDGFA theory (i.e. the Rayleigh normalized forward scattered intensity) Eq. (30), for DLCA soot aggregates versus the number of monomers per aggregate, N, for monomer radii of a = 15 and 30 nm and $\lambda = 600$ nm light, hence monomer size parameters ka = 0.157 and 0.314, respectively. These plots show a weak functionality of the deviation with N as well as functionalities on refractive index and size parameter. In general the smaller size parameter shows smaller deviations from RDGFA theory of approximately + 3% to +15% than the larger size parameter of approximately +20% to – 7%. We remark that a soot monomer radius of 15 nm is typical, whereas 30 nm is unusually large.

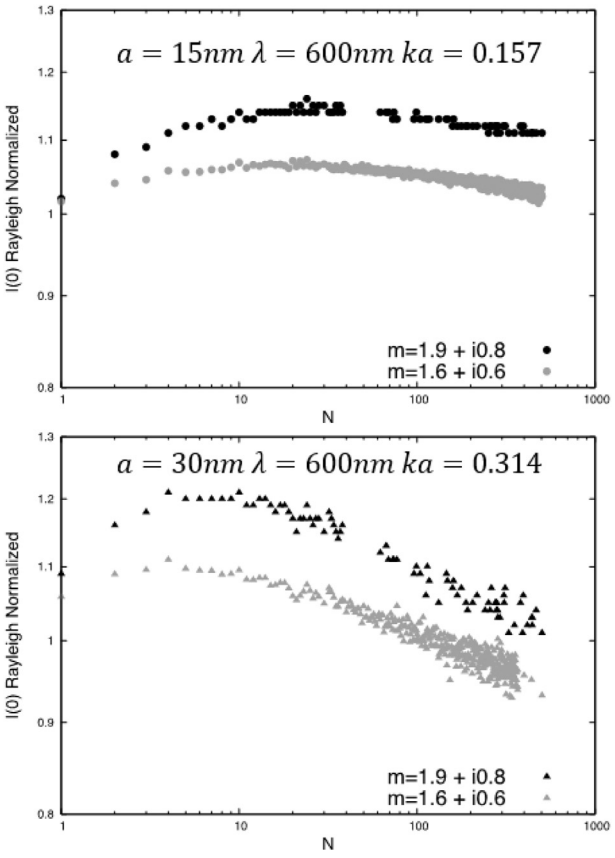

Fig. 9. Rayleigh normalized forward scattering intensities normalized by the RDGFA prediction versus the number of monomers in the aggregate N for soot DLCA aggregates composed of monomers with size parameters of $ka = 0.157$ (top) and 0.314 (bottom). The monomers have two representative refractive indices for soot as indicated in the key.

8.2. Light absorption

Fig. 10 shows the deviations of the light absorption cross section from the RDGFA theory (i.e. the Rayleigh normalized absorption cross section) Eq. (32), for DLCA soot aggregates versus the number of monomers per aggregate, N, for monomer radii of a = 15 and 30 nm and $\lambda = 600$ nm light, hence monomer size parameters ka = 0.157 and 0.314, respectively. As for scattering, these plots show a weak functionality of the deviation with N as well as functionalities on refractive index and size parameter. In general the smaller size parameter shows smaller deviations from RDGFA theory of approximately +3% to +23% than the larger size parameter of approximately +2% to 32%.

9. Aggregates with soot-like refractive index dispersion

The results reported in Figs. 9 and 10 show the strong impact of the refractive index on the degree of deviation from the RDG limit, i.e., the internal multiple scattering effects. Although various efforts have been made to investigate the soot refractive index and its wavelength dependence in the visible and near infrared spectrum, there are still relatively large uncertainties in the soot refractive index and its wavelength dependence has been commonly neglected in modeling studies or laser-based diagnostics of soot. However, it must be noticed that the refractive index of soot indeed displays wavelength dependence (dispersion) in the near UV–visible spectral range. In a recent study [46] optical refractive indices and their spectral dependency in the near UV-visible have been determined for different sources of particles, and it was found that three main compositions of the particles could encompass the observed broad range of the optical refractive indices found in the literature. The corresponding three compositions are considered here, namely graphitic, amorphous and organic composition for seven wavelengths covering the spectral domain 266–1064 nm. The organic soot exhibits the strongest spectral dependence. The amorphous soot presents a weak spectral dependence and low E(m) and F(m) values. The graphitic soot, which corresponds to mature soot, also presents a fairly weak spectral dependence similar to that of the amorphous soot case, but the graphitic soot presents larger values of E(m) and F(m). The corresponding optical refractive indices are reported in Table 1 as a function of the wavelengths, the reader is invited to consult [46] for more information concerning the determination of these refractive indices.

Three aggregates are considered for the calculations containing respectively N = 200, 284 and 833 primary spheres. The first one was tailor made ($D_f = 1.8$, $k_0 = 1.3$), the last two were generated by a DLCA code.

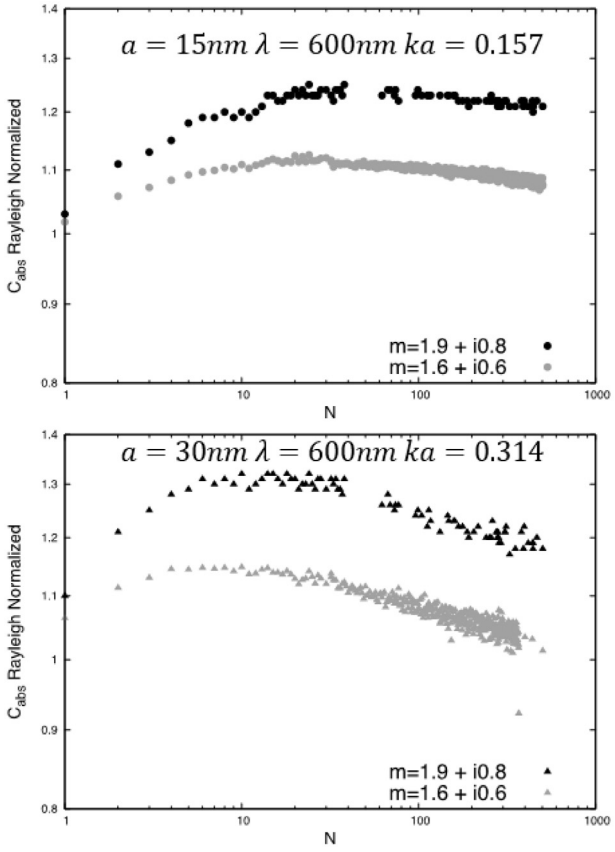

Fig. 10. Rayleigh normalized absorption cross section versus the number of monomers in the aggregate N for soot DLCA aggregates composed of monomers with size parameters of $ka = 0.157$ (top) and 0.314 (bottom). The monomers have two representative refractive indices for soot as indicated in the legend.

Table 1
Optical refractive indices for three different soot materials for a range of wave lengths, λ.

Composition	Graphitic		Amorphous		Organic	
$m = n + i\kappa$	n	κ	n	κ	n	κ
λ = 266 nm	1.02	0.64	1.06	0.46	0.94	0.96
λ = 354 nm	1.21	0.75	1.22	0.48	1.54	1.01
λ = 442 nm	1.35	0.80	1.32	0.46	1.83	0.75
λ = 532 nm	1.45	0.82	1.37	0.44	1.89	0.55
λ = 632 nm	1.53	0.84	1.41	0.42	1.89	0.42
λ = 848 nm	1.64	0.90	1.45	0.42	1.86	0.30
λ = 1064 nm	1.73	0.98	1.47	0.44	1.83	0.26

9.1. *Forward scattering functionality vs λ*

Fig. 11 presents the Rayleigh normalized forward scattering as a function of the wavelength for the three soot materials in Table 1 and three aggregate sizes N. Amorphous and graphitic compounds produce similar results, showing a significant overestimation of the forward scattering by the RDGFA theory (hence I(0) Rayleigh normalized is less than 1.0) at shorter wavelengths below 500 nm and a quite good prediction for $\lambda > 500$ nm. On the other hand, even at longer wavelengths, RDGFA poorly predicted the forward scattering by aggregates formed by the organic material (overestimation up to 50% of at 266 nm and underestimation up to 20% of at 532 nm). We observe that a physically acceptable spectral variation of the optical refractive index can strongly affect the internal multiple scattering effects hence deviations from RDGFA theory. In comparison to the observed variations caused by the refractive indices dispersion, the impact of the primary sphere diameter and number of primary particles in the aggregate appears to be secondary.

In our study of fractal aggregate scattering, Section 6.1 above, we found that the real part of the refractive index caused positive deviations form RDGFA theory whereas the imaginary part caused negative deviations. With this perspective, the large negative deviations for the soot materials here can be ascribed to the small real refractive indices combined with the large imaginary parts that occur at small wavelengths, see Table 1.

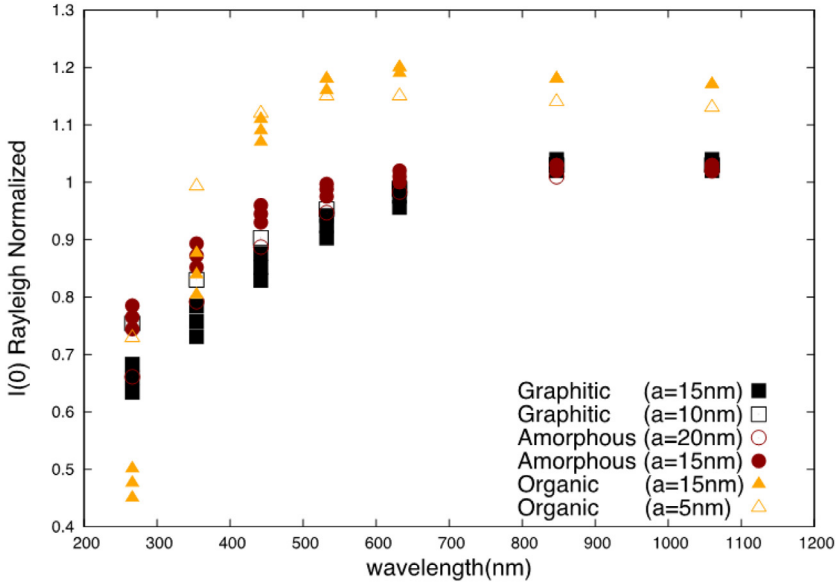

Fig. 11. Rayleigh normalized forward scattering intensities (i.e. normalized by the RDGFA prediction) versus the wavelength λ for three soot aggregates composed of $N = 200$, 284 and 833 monomers for three dispersion laws (Graphitic, Amorphous and Organic, Table 1). The filled symbols correspond to primary sphere radii of 15 nm, empty symbols corresponds to other primary sphere radii from 5 to 20 nm as indicated in the legend.

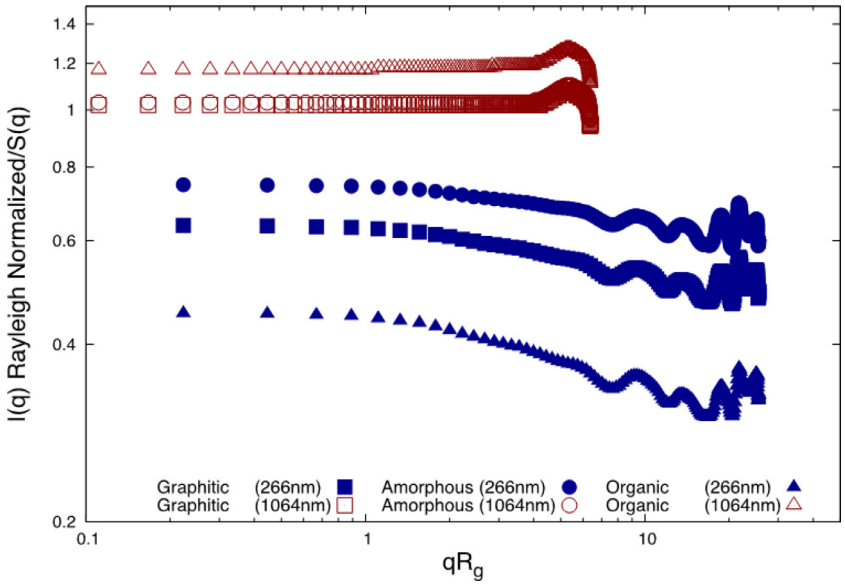

Fig. 12. Rayleigh normalized scattered intensity divided by the structure factor, ratio (31), for a DLCA soot aggregate composed of $N = 833$ monomers for three dispersion laws (Graphitic, Amorphous and Organic). The reported results corresponds to $\lambda = 266$ and 1064 nm for $a = 15$ nm.

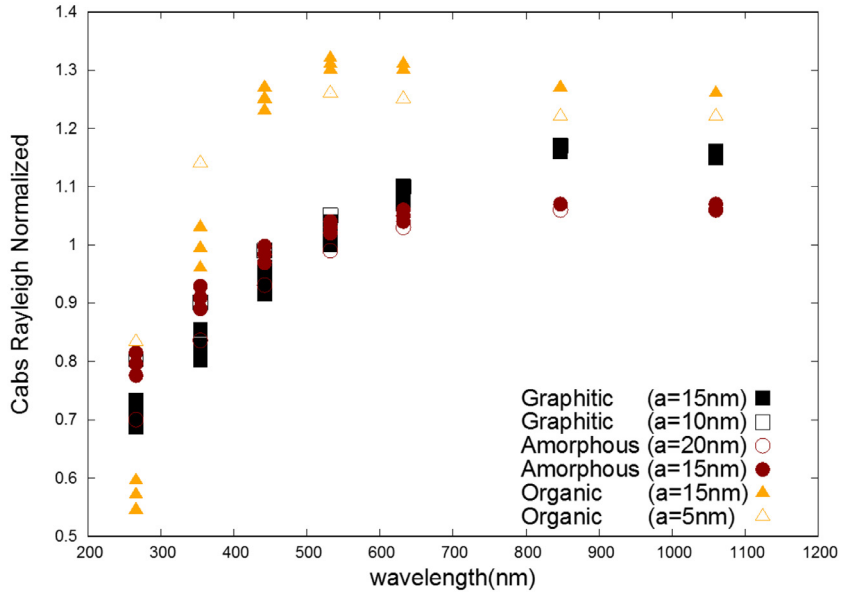

Fig. 13. Rayleigh normalized absorption cross section (i.e. normalized by the RDGFA prediction) versus the wavelength λ for three soot aggregates composed of N = 200, 284 and 833 monomers for three dispersion laws (Graphitic, Amorphous and Organic, Table 1). The filled symbols correspond to primary sphere radii of 15 nm, empty symbols corresponds to other primary sphere radii from 5 to 20 nm as indicated in the key.

We remark that attempts to use the internal coupling parameter ρ' to unify the description of the forward scattering by these three soots did not yield significant success.

9.2. Scattering functionality vs q

Fig. 12 presents the angular dependence of the Rayleigh normalized scattering divided by the structure factor, the ratio (31), for two wavelengths $\lambda = 266$ and 1064 nm. The structure factor was determined by performing DDA calculations for $m = 1.001 + i0.001$. Such calculations are in excellent agreement with those obtained by Fourier transformation of the pair autocorrelation functions. The ratio in Fig. 12 is the same ratio plotted in Figs. 5 and 6. For the considered aggregate (N = 833), at 1064 nm, except at largest q, the normalized scattered intensity is quite constant indicating that the angular dependency of the scattered light is represented well by the structure factor. As a consequence, the determination of the gyration radius in the Guinier regime and the fractal dimension in the power law regime will not suffer from the effects of internal multiple scattering at this wavelength. Only the amplitude of the signal is overestimated as discussed before. This is in accordance with conclusion made when commenting on Fig. 6. On the contrary, Fig. 12 shows that when $\lambda = 266$ nm, for the same aggregate, a progressive decrease of the curves for increasing q in the power law regime. That quite linear decrease in a log-log plot can affect the power law regime and thus the determination of the fractal dimension. Indeed, the slope of the scattered intensity in the region $1.56 < qR_g < 3.11$ (not presented) is shown to be −1.76 for $\lambda = 1064$ nm whereas it becomes at $\lambda = 266$ nm −1.81, −1.83 and −1.87, respectively, for amorphous, graphitic and organic materials.

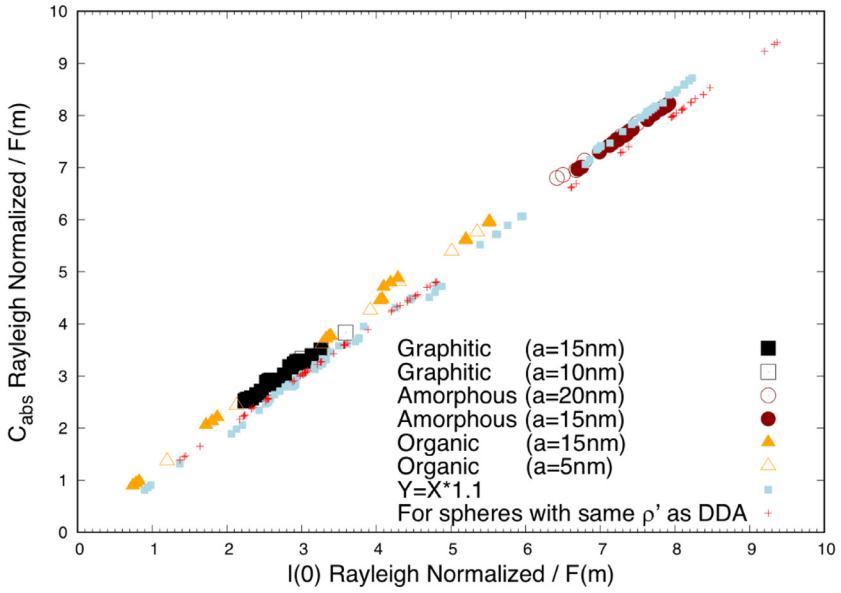

Fig. 14. Rayleigh normalized absorption cross section divided by F(m) versus Rayleigh normalized forward scattering cross section divided by F(m) for three soot aggregates composed of $N = 200$, 284 and 833 monomers and for three dispersion laws (Graphitic, Amorphous and Organic). The filled symbols correspond to primary sphere radii of 15 nm, empty symbols corresponds to other primary sphere radii from 5 to 20 nm as indicated in the key. Red crosses corresponds to spherical evaluation (Mie theory) based on the same internal coupling parameters than for considered aggregates, wavelengths and optical indices. (For interpretation of the references to color in this figure legend, the reader is referred to the web version of this article.)

This corresponds to an overestimation of the fractal dimension up to 6% at 266 nm for organic particles.

We now refer back to Fig. 6 which indicated that when the imaginary part of the refractive index was large, the apparent fractal dimension would be larger than the true value. This is seen again in Fig. 12 but augmented by the fact for these realistic soots the real part is quite small when $\lambda = 266$ nm. Then recalling our discussion of Fig. 11 we conclude that combination of small real part and large imaginary parts of the refractive index yield the greatest deviations from RDGFA theory.

9.3. Light absorption

Fig. 13 presents the Rayleigh normalized absorption cross section as a function of the wavelength for the three considered dispersion laws and three aggregate sizes N. The trends seen for scattering displayed in Fig. 11 are seen again for absorption and thus similar conclusions can be made.

A strong correlation between the correction to RDGFA for absorption and forward scattering, suggested by Figs. 11 and 13, has been observed for soot fractal aggregates by [12,16,18] who reported that the RDG normalized Cabs (h) is ≈1.1times the RDG normalized forward scattering (A). Fig. 14 illustrates that relationship for the three soot aggregates considered here, with different primary sphere diameters, seven wavelengths, and the corresponding optical refractive indices listed in Table 1. In Fig. 14 the absorption cross sections normalized by RDG and by F(m) is plotted as a function of forward scattering cross section also normalized by RDG expression and by F(m). For all the wavelengths, primary sphere radii and refractive indices considered, that figure demonstrates a linear relationship. The previously reported relationship $h = 1.11$A is also reported in filled blue boxes showing a good agreement with the present new results. Finally, the red crosses represent the same relationship determined for spheres (Mie theory) with identical wavelengths, optical indices and ρ' parameter (by adjusting the diameter). It appears that the deviations from RDG to absorption and scattering caused by internal coupling are strongly correlated for both aggregates and for spheres and that the scattering efficiency F(m) plays an important role in the internal multiple scattering.

10. Conclusions

We studied scattering and absorption by DLCA fractal aggregates with monodisperse monomers having point contacts. Deviations from the RDGFA theory for both scattering and absorption were found to be very similar, ranging as large as +25% for monomer size parameters of $ka = 0.157$ and +35% for ka = 0.314. Positive deviations increase with the real part of the refractive index and negative deviations grow with the imaginary part. Positive deviations dominate but these two parts tend to fight each other. The deviations increase with N in the first decade $1 \leq N \leq 10$ (very little deviation at $N = 1$) and then roughly level off, although the deviations decrease and can become negative with increasing N when the imaginary refractive index is large. These deviations from the RDG limit are similar to deviations for spheres, and in this context the internal coupling parameter provides some unifying description. Minor angular deviations from the structure factor shape also occur for large imaginary parts.

We believe that it would be useful for future studies to consider the effects of the fractal parameters, fractal dimension and prefactor, on the scattering and absorption relative to the RDGFA theory. Another valuable topic would be scattering and absorption by hybrid aggregate structures such as superaggregates formed in dense systems near the gel point [47–49].

Declaration of interests

None.

Acknowledgments

This work was supported by the U.S. Army Research Office (W911NF-15-1-0549) and the National Science Foundation (AGS1649783, AGS1665456, AGS1455215). The authors thank the

CRIANN for the computational resources provided by the Normandie region (France) and the BIOENGINE project co-financed by the European Union with the European regional development fund (ERDF) and by the Normandie Regional Council. FL thanks NRCan PERD for the financial support through TR3 Project 3B03.0002B.

Appendix. Theoretical basis of the RDG approximation for fractal aggregates

This appendix demonstrates how the RDGFA is obtained as an approximate solution to the Maxwell equations for a soot fractal aggregate and discusses several important limitations of that approximation. To begin, consider a single, spherical monomer of radius a and refractive index m. The monomer is located at the origin and a plane wave travelling along the unit vector $\hat{\mathbf{z}}$ illuminates the monomer. To begin with, regard the polarization direction of this incident wave as arbitrary given by the unit vector $\hat{\mathbf{e}}_o$, where $\hat{\mathbf{e}}_o \in \mathbb{C}^3$. This unit vector makes an angle ϕ with the positive x-axis. Thus, the incident electric field is given by

$$\mathbf{E}^{\text{inc}}(\mathbf{r}) = \hat{\mathbf{e}}_o E_o e^{ik\mathbf{r}\cdot\hat{\mathbf{z}}}, \tag{A1}$$

where E_o is the amplitude of the incident field. The Maxwell equations are solved for the scattered field in the monomer's far-field zone by the volume integral equation (VIE) as

$$\mathbf{E}_{\text{m}}^{\text{sca}}(\mathbf{r}) = \frac{k^2}{4\pi}\frac{e^{ikr}}{r}\left(m^2-1\right)\left(\overleftrightarrow{\mathbf{I}} - \hat{\boldsymbol{\mathfrak{r}}}\otimes\hat{\boldsymbol{\mathfrak{r}}}\right)\cdot\int_{V_m}\mathbf{E}_{\text{m}}^{\text{int}}(\mathbf{r}')e^{-ik\mathbf{r}'\cdot\hat{\mathbf{r}}}\text{d}v', \tag{A2}$$

where $\mathbf{E}_{\text{m}}^{\text{int}}$ is the internal field inside the monomer, V_{m} is the (spherical) monomer volume, $\boldsymbol{\mathfrak{r}} = \mathbf{r} - \mathbf{r}'$, and $\overleftrightarrow{\mathbf{I}}$ is the identity dyad [50]. In general, the internal field is not known *a priori* although in this case Mie theory could be used to find it because the monomer is spherical.

The RDGFA approximation begins with the recognition that the monomer is much smaller than the wavelength λ of the incident light. This means that the field responsible for polarizing the monomer material appears approximately uniform. Then, the internal field in Eq. (A2) can be approximated by the field inside a spherical particle placed in a uniform external field as [51].

$$\mathbf{E}_{\text{m}}^{\text{int}}(\mathbf{r}) = \hat{\mathbf{e}}_o\left(\frac{3}{m^2+2}\right)E_o e^{ik\mathbf{r}\cdot\hat{\mathbf{z}}},$$

or because the monomer is centered at the origin and $ka \ll 1$, the exponential here is $e^{(ikr\cdot\hat{z})} \cong 1$ throughout V_{m} and thus,

$$\mathbf{E}_{\text{m}}^{\text{int}}(\mathbf{r}) = \hat{\mathbf{e}}_o\left(\frac{3}{m^2+2}\right)E_o, \tag{A3}$$

which is itself a uniform field. Meanwhile, the scattered field is conveniently represented by a scattering amplitude $\mathbf{E}_1^{\text{sca}}$ as

$$\mathbf{E}_{\text{m}}^{\text{sca}}(\mathbf{r}) = \frac{e^{ikr}}{r}\mathbf{E}_1^{\text{sca}}\left(\hat{\mathbf{r}}\right) \tag{A4}$$

such that the amplitude only has dependence on the direction $\hat{\mathbf{r}}$ to the observation point. Then, combining Eqs. (A2) and (A3) and taking $\boldsymbol{\mathfrak{r}} \cong \mathbf{r}$ in the far-field zone shows that the scattering amplitude in Eq. (A4) is

$$\mathbf{E}_1^{\text{sca}}\left(\hat{\mathbf{r}}\right) = \frac{3k^2}{4\pi}\frac{m^2-1}{m^2+2}E_o\left(\overleftrightarrow{\mathbf{I}} - \hat{\mathbf{r}}\otimes\hat{\mathbf{r}}\right)\cdot\hat{\mathbf{e}}_o\int_{V_{\text{m}}}e^{-ik\mathbf{r}'\cdot\hat{\mathbf{r}}}\,\text{d}v'. \tag{A5}$$

However, the same approximation used to arrive at Eq. (A3) also means that $e^{-ikr'\cdot\hat{r}} \cong 1$ here in which case the integral is simply the monomer volume V_{m} and Eq. (A5) simplifies to

$$\mathbf{E}_1^{\text{sca}}\left(\hat{\mathbf{r}}\right) = k^2a^3E_o\frac{m^2-1}{m^2+2}\left[\hat{\mathbf{e}}_o - \left(\hat{\mathbf{e}}_o\cdot\hat{\mathbf{r}}\right)\hat{\mathbf{r}}\right]. \tag{A6}$$

Eq. (A6) is the Rayleigh scattering amplitude for a single monomer at the origin. From the transverse character of the far-field scattered wave, the scattered magnetic field is

$$\mathbf{B}_{\text{m}}^{\text{sca}}(\mathbf{r}) = \frac{1}{c}\frac{e^{ikr}}{r}\hat{\mathbf{r}}\times\mathbf{E}_1^{\text{sca}}\left(\hat{\mathbf{r}}\right), \tag{A7}$$

and the Rayleigh scattered intensity for the monomer $I_{\text{m}}(\mathbf{r})$ can be calculated as the magnitude of the time averaged Poynting vector $\langle\mathbf{S}\rangle_t = (1/2\mu_o)\text{Re}\{\mathbf{E}_{\text{m}}^{\text{sca}}\times[\mathbf{B}_{\text{m}}^{\text{sca}}]^*\}$ giving

$$I_{\text{m}}(\mathbf{r}) = \frac{k^4a^6|E_o|^2}{2\mu_o cr^2}F(m)\left(1 - \left|\hat{\mathbf{e}}_o\cdot\hat{\mathbf{r}}\right|^2\right), \tag{A8}$$

where $F(m)$ is the Lorentz-Lorenz factor of Eq. (13), and the identity $[\hat{\mathbf{e}}_o - (\hat{\mathbf{e}}_o\cdot\hat{\mathbf{r}})\hat{\mathbf{r}}]\cdot[\hat{\mathbf{e}}_o - (\hat{\mathbf{e}}_o\cdot\hat{\mathbf{r}})\hat{\mathbf{r}}]^* = 1 - |\hat{\mathbf{e}}_o\cdot\hat{\mathbf{r}}|^2$ is used where the asterisk denotes complex conjugation. With Eq. (A8), the Rayleigh differential scattering cross section can be found as

$$\frac{dC_{\text{m}}^{\text{sca}}}{d\Omega}\left(\hat{\mathbf{r}}\right) = r^2\frac{I_{\text{m}}(\mathbf{r})}{I^{\text{inc}}} = k^4a^6F(m)\left(1 - \left|\hat{\mathbf{e}}_o\cdot\hat{\mathbf{r}}\right|^2\right), \tag{A9}$$

where I^{inc} is the intensity of the incident wave. This result is the generalization of Eq. (12) for arbitrary polarization. For an incident wave linearly polarized along the x-axis, Eq. (A9) gives the scattering cross section for the monomer in the Rayleigh approximation as

$$C_{\text{m}}^{\text{sca}} = \int_{4\pi}\frac{dC_{\text{m}}^{\text{sca}}}{d\Omega}\left(\hat{\mathbf{r}}\right)d\Omega = \frac{8\pi}{3}k^4a^6F(m) \tag{A10}$$

where $\hat{\mathbf{e}}_o = \hat{\mathbf{x}}$ and $\hat{\mathbf{x}}\cdot\hat{\mathbf{r}} = \sin\theta\cos\phi$ is used. This result agrees with that in [1]. From the optical theorem [52], the monomer's extinction cross section is given by

$$C_{\text{m}}^{\text{ext}} = \frac{4\pi}{k|E_o|^2}\text{Im}\left\{E_o^*\hat{\mathbf{e}}_o^*\cdot\mathbf{E}_1^{\text{sca}}\left(\hat{\mathbf{z}}\right)\right\}. \tag{A11}$$

With Eq. (A6) in mind, one can see that Eq. (A11) gives a result that is not consistent with energy conservation. To see why, suppose that the monomer is non-absorbing for a given λ. Then, m is a pure real number and the imaginary filter in Eq. (A11) will return value of $C_{\text{m}}^{\text{ext}} = 0$ for a linearly polarized incident wave. Meanwhile the absorption cross section $C_{\text{m}}^{\text{abs}}$ is zero by definition as m has no imaginary part. Conservation of energy requires that $C_{\text{m}}^{\text{ext}} = C_{\text{m}}^{\text{abs}} + C_{\text{m}}^{\text{sca}}$, which shows that $C_{\text{m}}^{\text{sca}}$ should also be zero in this case. However, this is contradicted by the Rayleigh scattering cross section, Eq. (A10), and its relative, Eq. (12), as those expressions would give a nonzero value for $C_{\text{m}}^{\text{sca}}$. The error here is not in the optical theorem, which is perfectly valid in the far-field zone [52]. Rather, it is the assumption in the Rayleigh approximation that the monomer's internal field can be treated electrostatically.

A hallmark of the RDGFA approximation is that the differential scattering cross section for an *aggregate* of N identical spherical monomers is given by $S(q)$ times $dC_{\text{m}}^{\text{sca}}/d\Omega$, i.e., Eq. (10). To obtain this simple result from the VIE formally requires two approximations. The first is the Rayleigh approximation at the monomer level used above, i.e., that for each spherical monomer, $a \ll \lambda$ such that the polarization of the monomer material can be described electrostatically by the Lorentz-Lorenz factor. The second approximation applies at the aggregate level and relates to the interaction between monomers. If such interactions are neglected, i.e., multiple scattering between monomers is ignored, then the internal field of any given monomer will be determined by the incident field evaluated at the location of that monomer. Together these approximations are the gist of the RDGFA. Because the aggregate may be on the order of λ in size or greater, the phase of the incident field must now be accounted for. Thus, Eqs. (A1) and (A3) combine to give the i^{th} monomer's internal field as

$$\mathbf{E}_i^{\text{int}}(\mathbf{r}) = \hat{\mathbf{e}}_o\left(\frac{3}{m^2+2}\right)E_o e^{ik\mathbf{r}_i\cdot\hat{\mathbf{z}}}, \tag{A12}$$

where $\mathbf{r}_i$ is the location of the center of the i^{th} monomer in the aggregate.

To simplify the following, take the incident wave to be linearly polarized along the x-axis such that $\hat{\mathbf{e}}_o = \hat{\mathbf{x}}$ and focus specifically on how the aggregate scatters into the forward direction. Then, using Eq. (A2) the aggregate's forward-scattered field in the far-field zone is

$$\mathbf{E}^{\text{sca}}(z\hat{\mathbf{z}}) = \frac{k^2}{4\pi}\frac{e^{ikr}}{r}(m^2-1)\left(\overleftrightarrow{\mathbf{I}} - \hat{\mathbf{z}}\otimes\hat{\mathbf{z}}\right)\cdot\sum_{i=1}^{N}\int_{V_m}\mathbf{E}_i^{\text{int}}(\mathbf{r}')e^{-ik\mathbf{r}'\cdot\hat{\mathbf{z}}}\,\mathrm{d}v', \tag{A13}$$

Installing Eq. (A12) in Eq. (A13) and simplifying the dyadic product gives

$$\mathbf{E}^{\text{sca}}(z\hat{\mathbf{z}}) = \frac{3k^2}{4\pi}\frac{e^{ikr}}{r}\left(\frac{m^2-1}{m^2+2}\right)E_o\sum_{i=1}^{N}\int_{V_m}e^{ik\mathbf{r}_i\cdot\hat{\mathbf{z}}}e^{-ik\mathbf{r}'\cdot\hat{\mathbf{z}}}\mathrm{d}v'\;\hat{\mathbf{x}}. \tag{A14}$$

Because the internal field is constant inside each monomer, the substitution $\mathbf{r}' = \mathbf{r}_i$ can be made in the second exponential. Next, the scattering wave vector $\mathbf{q}(\hat{\mathbf{r}}) = k(\hat{\mathbf{z}} - \hat{\mathbf{r}})$ can be introduced, which in the forward direction is simply $\mathbf{q}(\hat{\mathbf{z}}) = 0$. However, $\mathbf{q}(\hat{\mathbf{z}})$ will continue to be shown to reveal Fourier-transform form of the end result. With regard to the integral in Eq. (A14), the small size of each monomer ($ka \ll 1$) means that the exponential approximately constant throughout V_m and can be brought out of the integral, i.e.,

$$\mathbf{E}^{\text{sca}}(z\hat{\mathbf{z}}) = \frac{3k^2}{4\pi}\frac{e^{ikr}}{r}\left(\frac{m^2-1}{m^2+2}\right)E_o\sum_{i=1}^{N}e^{i\mathbf{q}(\hat{\mathbf{z}})\cdot\mathbf{r}_i}\int_{V_m}\mathrm{d}v'\;\hat{\mathbf{x}}.$$

Finally, the integral can be evaluated to give

$$\mathbf{E}^{\text{sca}}(z\hat{\mathbf{z}}) = \frac{3k^2}{4\pi}\frac{e^{ikr}}{r}\left(\frac{m^2-1}{m^2+2}\right)E_oV_m\sum_{i=1}^{N}e^{i\mathbf{q}(\hat{\mathbf{z}})\cdot\mathbf{r}_i}\hat{\mathbf{x}} \tag{A15}$$

In close analogy to Eq. (7), define the aggregate structure factor in the forward direction as

$$S(\hat{\mathbf{z}}) = \frac{1}{N^2}\left|\sum_{i=1}^{N}e^{i\mathbf{q}(\hat{\mathbf{z}})\cdot\mathbf{r}_i}\right|^2. \tag{A16}$$

Again because the far-field scattered fields are transverse, the scattered magnetic field can be found from Eqs. (A4), (A7), and (A15) to get the time averaged scattered Poynting vector $\langle\mathbf{S}\rangle_t$. From $\langle\mathbf{S}\rangle_t$ and Eq. (A9), the differential scattering cross section for the aggregate in the forward direction becomes

$$\frac{dC_{\text{agg}}^{\text{sca}}}{d\Omega}(\hat{\mathbf{z}}) = \frac{9k^4}{16\pi^2}V_m^2N^2F(m)S(\hat{\mathbf{z}}). \tag{A17}$$

However, from Eq. (A16) one can see that $S(\hat{\mathbf{z}}) = 1$ because $\mathbf{q}(\hat{\mathbf{z}}) = 0$ so Eq. (A17) becomes

$$\frac{dC_{\text{agg}}^{\text{sca}}}{d\Omega}(\hat{\mathbf{z}}) = k^4a^6N^2F(m) \tag{A18}$$

in agreement with Eq. (17). Lastly, note that the aggregates scattered intensity for *any* angle can also be expressed in terms of the structure factor. To do so requires replacing $(\overleftrightarrow{\mathbf{I}} - \hat{\mathbf{z}}\otimes\hat{\mathbf{z}})$ in Eq. (A13) by $(\overleftrightarrow{\mathbf{I}} - \hat{\mathbf{r}}\otimes\hat{\mathbf{r}})$ of Eq. (A5) while the simplifications of the exponentials following Eq. (A14) may still be made.

References

[1] Sorensen CM. Light scattering by fractal aggregates: a review. Aerosol Sci Technol 2001;35:648–87.
[2] Meakin P. Formation of fractal clusters and networks by irreversible diffusion-limited aggregation. Phys Rev Lett 1983;51:1119–22.
[3] Kolb M, Botet R, Jullien R. Scaling of kinetically growing clusters. Phys Rev Lett 1983;51:1123–6.
[4] Sorensen CM, Roberts GC. The prefactor of fractal aggregates. J Colloid Interf Sci 1997;186:447–52.
[5] Lattuada M, Wu H, Morbidelli M. A simple model for the structure of fractal aggregates. J Colloid Interf Sci 2003;268:106–20.
[6] Heinson WR, Sorensen CM, Chakrabarti A. A three parameter description of the structure of diffusion limited cluster fractal aggregates. J Colloid Interf Sci 2012;375:65–9.
[7] Liu L, Mishchenko MI. Scattering and radiative properties of complex soot and soot-containing aggregate particles. J Quant Spectrosc Radiat Transfer 2007;106:262–73.
[8] Liu L, Mishchenko MI, Arnott WP. A study of radiative properties of fractal soot aggregates using the superposition t-matrix method. J Quant Spectrosc Radiat Transfer 2008;109:2656–63.
[9] Liu FS, Wong C, Snelling DR, Smallwood GJ. Investigation of absorption and scattering properties of soot aggregates of different fractal dimension at 532nm using rdg and gmm. Aerosol Sci Technol 2013;47:1393–405.
[10] Doner N, Liu FS. Impact of morphology on the radiative properties of fractal soot aggregates. J Quant Spectrosc Radiat Transfer 2017;187:10–19.
[11] Doner N, Liu FS, Yon J. Impact of necking and overlapping on radiative properties of coated soot aggregates. Aerosol Sci Technol 2017;51:532–42.
[12] Yon J, Roze C, Girasole T, Coppalle A, Mees L. Extension of rdg-fa for scattering prediction of aggregates of soot taking into account interactions of large monomers. Part Part Syst Char 2008;25:54–67.
[13] Liu C, Yin Y, Hu F, Jin H, Sorensen CM. The effects of monomer size distribution on the radiative properties of black carbon aggregates. Aerosol Sci Technol 2015;49:928–40.
[14] Liu FS, Smallwood GJ. Effect of aggregation on the absorption cross-section of fractal soot aggregates and its impact on lii modelling. J Quant Spectrosc Radiat Transfer 2010;111:302–8.
[15] Liu F, Smallwood GJ. The effect of particle aggregation on the absorption and emission properties of mono- and polydisperse soot aggregates. Appl Phys B Lasers O 2011;104:343–55.
[16] Yon J, Liu FS, Bescond A, Caumont-Prim C, Roze C, Ouf FX, Coppalle A. Effects of multiple scattering on radiative properties of soot fractal aggregates. J Quant Spectrosc Radiat Transfer 2014;133:374–81.
[17] Prasanna S, Riviere P, Soufiani A. Effect of fractal parameters on absorption properties of soot in the infrared region. J Quant Spectrosc Radiat Trasfer 2014;148:141–55.
[18] Yon J, Bescond A, Liu F. On the radiative properties of soot aggregates part 1: necking and overlapping. J Quant Spectrosc Radiat Transfer 2015;162:197–206.
[19] Soewono A, Rogak SN. Morphology and optical properties of numerically simulated soot aggregates. Aerosol Sci Technol 2013;47:267–74.
[20] Liu FS, Yon J, Bescond A. On the radiative properties of soot aggregates - part 2: effects of coating. J Quant Spectrosc Radiat Transfer 2016;172:134–45.
[21] Berg MJ, Sorensen CM. Internal fields of soot fractal aggregates. J Opt Soc Am A 2013;30:1947–55.
[22] Mountain RD, Mulholland GW. Light-scattering from simulated smoke agglomerates. Langmuir 1988;4:1321–6.
[23] Sorensen CM, Cai J, Lu N. Test of static structure factors for describing light scattering from fractal soot aggregates. Langmuir 1992;8:2064–9.
[24] Heinson WR, Chakrabarti A, Sorensen CM. A new parameter to describe light scattering by an arbitrary sphere. Opt Commun 2015;356:612–15.
[25] Heinson YW, Maughan JB, Ding JC, Chakrabarti A, Yang P, Sorensen CM. Q-space analysis of light scattering by ice crystals. J Quant Spectrosc Radiat Transfer 2016;185:86–94.
[26] Maughan JB, Chakrabarti A, Sorensen CM. Rayleigh scattering and the internal coupling parameter for arbitrary particle shapes. J Quant Spectrosc Radiat Transfer 2017;189:339–43.
[27] Sorensen CM, Heinson YW, Heinson WR, Maughan JB, Chakrabarti A. Q-space analysis of the light scattering phase function of particles with any shape. Atmos. Basel 2017;8.
[28] Maughan JB, Chakrabarti A, Sorensen CM. Rayleigh scattering and the internal coupling parameter for arbitrary shapes. J Quant Spectrosc Radiat Transfer 2017;189:339–43.
[29] van de Hulst HC. Light scattering by small particles. New York: Wiley; 1957. p. 470. p.
[30] Kerker M. The scattering of light, and other electromagnetic radiation, New York: Academic Press; 1969. p xv, 666 p.
[31] Medalia AI. Morphology of aggregates .1. Calculation of shape and bulkiness factors - application to computer-simulated random flocs. J Colloid Interf Sci 1967;24:393–404.
[32] Medalia AI, Heckman FA. Morphology of aggregates .2. Size and shape factors of carbon black aggregates from electron microscopy. Carbon 1969;7:567–82.
[33] Oh C, Sorensen CM. The effect of overlap between monomers on the determination of fractal cluster morphology. J Colloid Interf Sci 1997;193:17–25.
[34] Pierce F, Sorensen CM, Chakrabarti A. Computer simulation of diffusion-limited cluster-cluster aggregation with an epstein drag force. Phys Rev E 2006;74:021411–18.
[35] Sorensen CM. The mobility of fractal aggregates: a review. Aerosol Sci Technol 2011;45:765–79.
[36] Filippov AV, Zurita M, Rosner DE. Fractal-like aggregates: relation between morphology and physical properties. J Colloid Interf Sci 2000;229:261–73.
[37] Liu F, Snelling DR. Evaluation of the accuracy of the rdg approximation for the absorption and scattering properties of fractal aggregates of flame-generated soot. 40th thermophysics conference, AIAA 2008-4362, Seattle, Washington; 2008.

[38] Mackowski DW, Mishchenko MI. A multiple sphere t-matrix fortran code for use on parallel computer clusters. J Quant Spectrosc Radiat Transfer 2011;112:2182–92.
[39] Draine BT, Flatau PJ. Discrete-dipole approximation for scattering calculations. J Opt Soc Am A 1994;11:1491–9.
[40] Brasil AM, Farias TL, Carvalho MG. Evaluation of the fractal properties of cluster-cluster aggregates. Aerosol Sci Technol 2000;33:440–54.
[41] Liu F, Snelling DR, Smallwood GJ. Effects of the fractal prefactor on the optical properties of fractal soot aggregates. In: Proceedings of MNHMT2009, ASME 2009 2nd micro/nanoscale heat & mass transfer international conference, Shanghai, China; 2009.
[42] Wang G, Chakrabarti A, Sorensen CM. Effect of the imaginary part of the refractive index on light scattering by spheres. J Opt Soc Am A 2015;32:1231–5.
[43] Dalzell WH, Sarofim AF. Optical constants of soot and their application to heat-flux calculations. J Heat Transf 1969;91:100–4.
[44] Smith FW. Optical-constants of a hydrogenated amorphous-carbon film. J Appl Phys 1984;55:764–71.
[45] Bond TC, Bergstrom RW. Light absorption by carbonaceous particles: an investigative review. Aerosol Sci Technol 2006;40:27–67.
[46] Bescond A, Yon J, Ouf FX, Roze C, Coppalle A, Parent P, Ferry D, Laffon C. Soot optical properties determined by analyzing extinction spectra in the visible near-uv: toward an optical speciation according to constituents and structure. J Aerosol Sci 2016;101:118–32.
[47] Sorensen CM, Kim W, Fry D, Shi D, Chakrabarti A. Observation of soot superaggregates with a fractal dimension of 2.6 in laminar acetylene/air diffusion flames. Langmuir 2003;19:7560–3.
[48] Kim W, Sorensen CM, Chakrabarti A. Universal occurrence of soot superaggregates with a fractal dimension of 2.6 in heavily sooting laminar diffusion flames. Langmuir 2004;20:3969–73.
[49] Sorensen CM, Chakrabarti A. The sol to gel transition in irreversible particulate systems. Soft Matter 2011;7:2284–96.
[50] Mishchenko MI, Travis LD, Lacis AA. Scattering, absorption and emission of light by small particles. Cambridge: Cambridge U. K.: Unniversity Press; 2002.
[51] Griffiths DJ. Introduction to electrodynamics. 3rd ed. NJ: Prentice Hall: Upper Saddler River; 1999. p xv, 576 p.
[52] Berg MJ, Sorensen CM, Chakrabarti A. Extinction and the optical theorem. Part i. Single particles. J Opt Soc Am A 2008;25:1504–13.